Investigation of deep sub-barrier fusion in asymmetric systems

Rohan Biswas[1,⋆], *S.* Nath[1,⋆⋆], *J.* Gehlot[1], *Gonika*[1], *Chandra* Kumar[1], *A.* Parihari[2,⋆⋆⋆], *N.* Madhavan[1], *A.* Vinayak[3], *Amritraj* Mahato[4], *Shoaib* Noor[5], and *Phurba* Sherpa[2]

[1] *Nuclear Physics Group, Inter-University Accelerator Centre, Aruna Asaf Ali Marg, New Delhi 110067, India*
[2] *Department of Physics & Astrophysics, Delhi University, Delhi 110007, India*
[3] *Department of Physics, Karnatak University, Dharwad 580003, India*
[4] *Department of Physics, Central University of Jharkhand, Ranchi 835205, India*
[5] *School of Physics & Materials Science, Thapar Institute of Engineering & Technology, Patiala 147004, India*

Abstract. Enhancement of fusion cross sections below the interaction barrier has been quite successfully explained by coupled-channels methods. However, extending the measurements to deep sub-barrier energies revealed a steeper descent of the excitation function which could not be explained by standard coupled-channels calculations. Though a large number of heavy-ion and light-ion induced reactions have been investigated to understand the dynamics of fusion deep below the barrier, the phenomenon of *fusion hindrance* has been studied only for a handful of asymmetric systems. We report new measurements of fusion excitation functions for the systems ^{16}O+^{116}Cd and ^{16}O+^{142}Ce. We also present comparisons of the same with the data for existing symmetric systems having nearly similar values of the ζ parameter, characterizing the size of the colliding system. We extracted the logarithmic derivatives of the energy-weighted cross sections and the astrophysical S-factors. Experimental results were reproduced well by coupled-channels calculations. We extrapolated our results, following the systematics, beyond the threshold energy for fusion hindrance for both the systems. From our investigation, we conclude that the present asymmetric systems, as well as the corresponding symmetric systems, show fusion hindrance and this feature is independent of the entrance channel mass asymmetry.

1 Introduction

Heavy ion-induced fusion reactions have been studied quite extensively over the last few decades. The measured fusion cross sections span orders of magnitude in their absolute value across the Coulomb barrier. The couplings of various internal degrees of freedom and other direct reaction channels with the relative motion between the nuclei in the entrance channel have been quite successful in explaining the substantial enhancement of fusion cross sections below the barrier [1–4]. However, a steeper reduction of fusion cross sections at lower energies could not be explained by standard coupled-channels calculations [5]. The phenomenon, termed as *fusion hindrance*, was first reported by Jiang *et al.* [6] for the system ^{60}Ni+^{89}Y. Since then, numerous heavy ion and light ion-induced fusion reactions have been studied to unravel the fusion dynamics deep below the barrier [7].

Analyzing the data from a large number of systems, major inferences on fusion hindrance have been drawn. Onset of fusion hindrance has been observed to occur at lower energies for the systems with open-shell ("soft") collision partners than the systems with closed-shell ("stiff") nuclei in the entrance channel [8, 9]. The effect of charge product of the participating nuclei (Z_1Z_2) on fusion hindrance [10, 11] shows that lighter systems are less likely to exhibit fusion hindrance in comparison with heavier systems. Studies on systems with small negative Q-value [12] and positive Q-value [13, 14] have also revealed fusion hindrance. It was thus established that heavy-ion fusion hindrance was a general phenomenon. Studies on various Ca+Zr systems revealed that presence of multiple PQNT channels could enhance fusion cross sections even in the deep sub-barrier region [15, 16]. Two representations have been introduced to determine the threshold energy at which fusion hindrance sets in [17]: (a) the logarithmic slope of the energy weighted fusion cross sections (discussed in Section 3.3) and (b) the astrophysical S-factor (discussed in Section 3.4). An empirical value of the threshold energy ($E_S^{\rm emp}$) had been estimated from the systematics, which is given as $E_S^{\rm emp} = 0.356\zeta^{2/3}$ [17]. Here, the parameter $\zeta = Z_1Z_2\sqrt{\mu}$, where μ is the reduced mass in the entrance channel. This empirical relation suggests that the energy at which hindrance sets in depends on the mass and charge of the collision partners.

The microscopic origin of fusion hindrance is still a matter of debate. Two models have been partly successful in explaining the phenomenon. The sudden model [18, 19]

⋆Present Address: Life Science Division, Diamond Light Source Ltd., Diamond House, Harwell Science and Innovation Campus, Didcot, Oxfordshire OX11 0DE, UK
⋆⋆e-mail: subir@iuac.res.in
⋆⋆⋆Present Address: Department of Physics, Rajdhani College, University of Delhi, Mahatma Gandhi Marg, Raja Garden, New Delhi 110015, India

considers a shallow potential, constructed from the double folding model, with a short-range repulsive core. The repulsive core originates from the incompressibility of infinite nuclear matter determined from the nuclear equation of state and Pauli principle. According to this model, fusion happens so suddenly that the density is doubled at the overlapping region of the two participating nuclei. The adiabatic model [20–22] considers fusion to happen slowly, smoothly transitioning under the influence of a two-body potential to a one-body potential. The smooth transition occurs due to damping of collective motions in the entrance channel, quenching the enhancement in the fusion cross sections. The Pauli exclusion principle has also been applied in a microscopic approach using density-constrained frozen Hartree Fock calculations [23], where it decreases the tunneling probability inside the Coulomb barrier, initiating fusion hindrance below the barrier. A similar explanation was proposed by Dasgupta *et al.* [24], in which the onset of gradual quantum decoherence could lead to fusion hindrance at energies deep below the barrier, rendering the coupled-channels (CC) formalism inadequate.

There exists a paucity of fusion cross section data in the deep sub-barrier region for asymmetric systems. The reasons stem from the difficulty in measuring such low cross sections using recoil separators. Measurements performed in normal kinematics at low projectile energies lead to very small evaporation residue (ER) kinetic energies, causing their detection quite a difficult task. Separation of the background is also a formidable challenge deep below the barrier. Study of fusion hindrance on the system ^{16}O+^{204,208}Pb [24] revealed that the standard CC calculations were unable to predict the experimental cross sections, at all energy regions around the barrier, using the same set of potential parameters. More asymmetric systems with weakly-bound stable projectiles such as ^{6,7}Li+^{198}Pt [25] were studied where fusion hindrance was not observed. As the mass of projectiles was increased, as in case of ^{12}C+^{198}Pt [11] and very recently, ^{16}O+^{165}Ho [26], hindrance was observed. An weak signature of hindrance was reported for the system ^{11}Be+^{197}Au [27]. The effect of breakup channels in the deep sub-barrier region was observed for the systems ^{8}B+^{208}Pb [28], where the projectile was a proton-halo nucleus, and also in the system ^{19}F+^{181}Ta [29], where the α-particle breakup threshold was lower than the projectiles ^{12}C and ^{16}O.

In this article, we report measurement of fusion cross sections for two asymmetric systems, *viz.*, ^{16}O+^{116}Cd and ^{16}O+^{142}Ce. The systems do not have any positive Q-value neutron transfer (PQNT) channels, which might enhance the fusion cross sections in the deep sub-barrier region. ^{16}O, being a doubly closed-shell nucleus, has a rather high α-particle breakup threshold of 7.162 MeV, hence the effect of break-up channels is least expected to affect the fusion cross sections below the barrier. We also investigated the effect of entrance channel mass asymmetry on fusion hindrance by comparing the results of the present systems with that of symmetric systems, obtained from the literature, having similar values of ζ. Thus, results of the asymmetric system ^{16}O+^{116}Cd (ζ = 1440) were compared with results from the symmetric systems ^{36}S+^{48}Ca (ζ = 1451) [30] and ^{32}S+^{48}Ca (ζ = 1402) [31]. Similarly, results of ^{16}O+^{142}Ce (ζ = 1760) were compared with that of ^{28}Si+^{64}Ni (ζ = 1730) [32] and ^{40}Ca+^{40}Ca (ζ = 1789) [33].

2 Experimental Details

The experiment was performed using the Heavy Ion Reaction Analyzer (HIRA) [34] at IUAC, New Delhi. A pulsed beam of ^{16}O ions, with a pulse separation of 4 μs, was obtained from the 15UD Pelletron accelerator. Isotopically enriched ^{116}Cd and ^{142}Ce thin films were used as targets. The ^{116}Cd target had a thickness of 20 μg/cm^2 with a carbon backing of ∼ 20 μg/cm^2 [35]. The ^{142}Ce target, having a thickness of ∼ 120 μg/cm^2, was sandwiched between carbon backing and capping layers with thicknesses of ∼ 20 μg/cm^2 and ∼ 5 μg/cm^2, respectively [36]. Beam energy ($E_{\rm lab}$) was varied between 42 –76 MeV, in steps of 1 MeV.

Two silicon detectors were placed at $\theta_{\rm lab}$ = 15° for beam monitoring and normalization at a distance of 100 mm from the target with a circular aperture of 1 mm diameter. The HIRA was operated at $\theta_{\rm lab}$ = 0° with an acceptance of 5 msr. A thin (∼ 10 μg/cm^2) graphite charge-reset foil was placed 10 cm downstream from the target. A Multi-Wire Proportional Counter (MWPC), with dimensions 150 mm (horizontal) and 50 mm (vertical), was placed at the focal plane of the HIRA. Pressure of isobutane gas inside the MWPC was maintained at 3 Torr. A Time-to-Amplitude Converter (TAC) was set up to obtain a measure of the time-of-flight (TOF) of the ERs, travelling from the target to the focal plane. The timing signal from the anode of the MWPC and the radiofrequency (RF) pulse, used for beam pulsing, were respectively used as the start and the stop of the TAC. The ERs produced in both reactions were unambiguously identified by the energy loss, obtained from the cathode of the MWPC, and the TOF signals.

We mention here that two more silicon detectors were placed at backward angles of $\theta_{\rm lab}$ = 138° and 150° inside the target chamber to detect back-scattered projectile-like ions. The HIRA was also used to measure the scattered target-like ions in the focal plane. Results from measurements of quasielastic events will be reported elsewhere. Here, we report results from fusion measurements of the systems ^{16}O+^{116}Cd,^{142}Ce.

3 Data Analysis and Results

Fusion cross section ($\sigma_{\rm fus}$) was extracted from measured yields, following the methodology prescribed in Ref. [37]. Transmission efficiency of the HIRA for ERs was calculated using the semi-microscopic Monte Carlo code TERS [38]. The isotopic abundances of both the targets [35, 36] were taken into account while calculating $\sigma_{\rm fus}$.

The fusion excitation functions of the systems ^{16}O+^{116}Cd and ^{16}O+^{142}Ce are shown in Figs. 1(a) and 1(b), respectively. The $\sigma_{\rm fus}$ of ^{16}O+^{142}Ce at the lowest

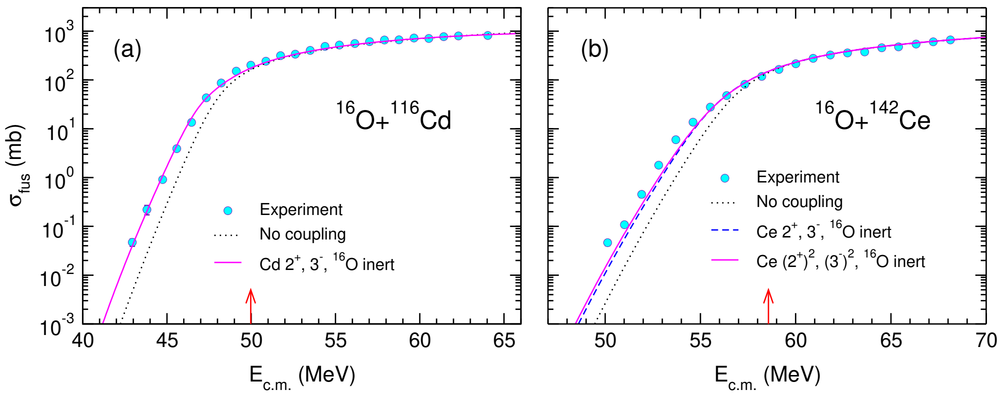

Figure 1: Fusion excitation functions for the systems (a) ^{16}O+^{116}Cd and (b) ^{16}O+^{142}Ce. The theoretical cross sections were calculated using the code CCFULL. Couplings included in the CC calculations are mentioned. The Coulomb barrier for each system is shown by a red arrow.

energy is slightly enhanced (as observed in Fig. 1(b)), possibly due to contamination of beam-like background in the ER yield. Segregating background from the events of interest became increasingly challenging with decreasing $E_{\rm lab}$. $\sigma_{\rm fus}$ could be measured down to $\simeq$ 14% below the barrier in the present experimental setup.

3.1 Fusion Barrier Distributions

The fusion barrier distribution ($\mathcal{D}$) was first extracted from the experimental $\sigma_{\rm fus}$, following the conventional double-differential method [39], using the point-difference formula. Taking the energy interval ΔE = 2 MeV smoothened the data and reduced the error in $\mathcal{D}$, since the same depends inversely on the square of ΔE. The $\mathcal{D}$ for ^{16}O+^{116}Cd and ^{16}O+^{142}Ce are shown in Fig. 2(a) and Fig. 2(b), respectively. The $\mathcal{D}$, in both systems, is fairly smooth and do not show any distinct feature which could be attributed to specific coupling to low-lying excited states in the entrance channel.

It can be observed that experimental $\mathcal{D}$ became poorly-defined with increasing energy (Fig. 2). In a recent article, Jiang *et al.* [40] pointed out that fusion $\mathcal{D}$ obtained from the "double-differentiation recipe" [39] was susceptible to ambiguities because of its dependence on the energy step size and large uncertainties in the extracted results. An alternative method to extract the *experimental* $\mathcal{D}$ from measured fusion excitation function had been suggested by Siwek-Wilczyńska *et al.* [41]. In this method, the barrier height distribution, as a function of the energy available in the centre of mass (c.m.) frame of reference (E), is assumed to be a Gaussian and $\sigma_{\rm fus}$ is expressed by a simple analytic function of the form

$$\sigma_{\rm fus}(E) = \frac{\sqrt{\pi}R_{\rm g}^2 W_{\rm g}}{\sqrt{2}E}\left[\sqrt{\pi}\,\mathcal{Z}\,{\rm erfc}(-\mathcal{Z}) + \exp\left(-\mathcal{Z}^2\right)\right], \quad (1)$$

with $\mathcal{Z} = (E - V_{\rm g})/\sqrt{2}W_{\rm g}$. Here, $V_{\rm g}$ and $W_{\rm g}$ are the centroid and the standard deviation of the Gaussian barrier distribution, respectively, and $R_{\rm g}$ is the barrier radius. Erfc is the complementary error function. A least-squares fit of the fusion excitation functions by Eq. 1 resulted in $V_{\rm g}$ = 47.108 MeV, $W_{\rm g}$ = 1.171 MeV and $R_{\rm g}$ = 10.396 fm with the associated χ^2 = 2.84 for the reaction ^{16}O+^{116}Cd. For ^{16}O+^{142}Ce, the corresponding values were 56.413 MeV, 1.975 MeV, 10.671 fm and 2.04, respectively.

3.2 Coupled-Channels Calculations

CC calculations were performed for the systems ^{16}O+^{116}Cd and ^{16}O+^{142}Ce using the code CCFULL [42] with the nuclear potential in the Woods-Saxon form. For ^{16}O+^{116}Cd, the potential parameters were: depth (V_0) = 58.4 MeV, reduced radius (r_0) = 1.17 fm and diffuseness parameter (a_0) = 0.78 fm. The parameters for ^{16}O+^{142}Ce were: V_0 = 99.5 MeV, r_0 = 1.20 fm and a_0 = 0.56 fm. The spectroscopic information of the low-lying collective excited states, λ^π, of the heavier collision partner in each case, with excitation energy, E_λ, and reduced deformation parameter, β_λ, are presented in Table 1.

Results of CC calculations, along with the fusion excitation functions and the corresponding $\mathcal{D}$s for both systems, are depicted in Fig. 1 and Fig. 2, respectively. In the calculations, when both collision partners were treated as structureless, the results expectedly underpredicted measured excitation functions in both cases, as shown in Fig. 1 (a) and (b). Next, for ^{16}O+^{116}Cd, we treated ^{16}O as inert while considering one-phonon excitation with mutual excitations for both the quadrupole (2^+) and the octopole (3^-) modes in ^{116}Cd. As a result, the theoretical cross sections showed enhancement in the sub-barrier re-

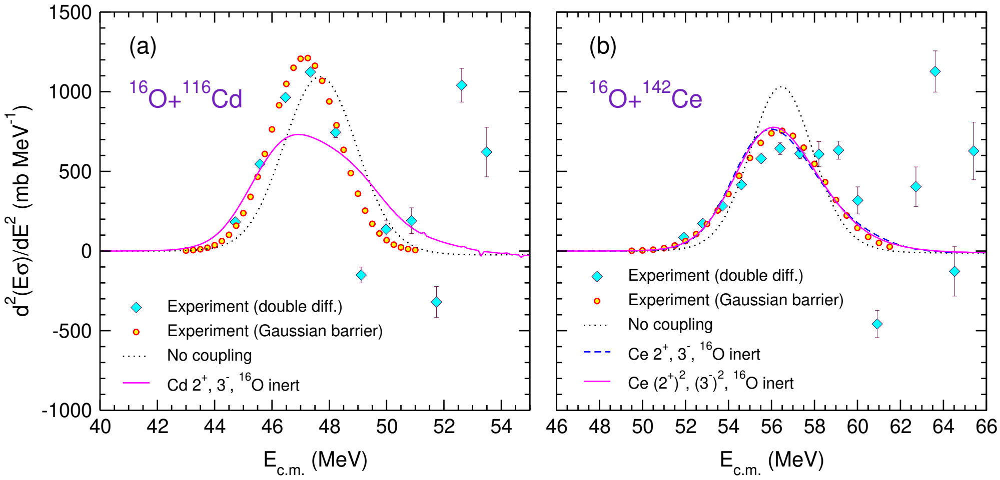

Figure 2: Experimental $\mathcal{D}$ for the systems (a) ^{16}O+^{116}Cd and (b) ^{16}O+^{142}Ce compared with results of CC calculations.

Table 1: Structural parameters of ^{116}Cd and ^{142}Ce [43, 44], denoted by their total angular momentum and parity (λ^{π}), excitation energy (E_{λ}) and reduced deformation parameter (β_{λ}).

Nucleus	λ^{π}	E_{λ} (MeV)	β_{λ}
^{116}Cd vib.	2^+	0.513	0.194
	3^-	1.922	0.138
^{142}Ce vib.	2^+	0.641	0.125
	3^-	1.653	0.132

gion (solid line in Fig. 1 (a)), which reproduced the data quite well. The corresponding $\mathcal{D}$ is shown in Fig. 2 (a). In case of ^{16}O+^{142}Ce also, we treated ^{16}O as inert and incorporated vibrational coupling of ^{142}Ce in the CC calculations. Initially, we considered one-phonon excitations for both the quadrupole (2^+) and the octopole (3^-) modes in ^{142}Ce. This led to a significant enhancement of cross sections in the sub-barrier region, though the theoretical result still underpredicted the experimental data. We further increased the number of phonons in the coupling scheme, including two-phonons with mutual excitations of both the quadrupole and the octupole modes, which caused marginal enhancement of theoretical cross sections, represented by the solid line in Fig. 1 (b). The corresponding $\mathcal{D}$s are shown in Fig. 2 (b). This coupling scheme for ^{16}O+^{142}Ce reproduced both the experimental excitation function and the experimental $\mathcal{D}$ reasonably well. Thus no hindrance to fusion was observed experimentally in both the systems down to the lowest $E_{\rm lab}$ at which measurements were performed.

3.3 Logarithmic Slopes

One of the representations to clearly observe fusion hindrance is the logarithmic slope, which can be computed from $\sigma_{\rm fus}$ using the relation

$$L(E) = \frac{d}{dE}\ln(\sigma_{\rm fus}E) = \frac{1}{\sigma_{\rm fus}E}\frac{d}{dE}(\sigma_{\rm fus}E)\ . \qquad (2)$$

$L(E)$ for the systems ^{16}O+^{116}Cd and ^{16}O+^{142}Ce are shown in Fig. 3(a) and Fig. 4(a), respectively. The logarithmic slopes at S-factor maximum ($L_{\rm CS}(E) = \pi\eta/E$), where $\eta = 0.1575\zeta/\sqrt{E}$ is the Sommerfeld parameter, are also shown in the figures (dot-dashed line). We observe from both figures that the experimental $L(E)$ does not reach the $L_{\rm CS}(E)$ curve. To extrapolate $L(E)$ beyond the lowest $E_{\rm lab}$, a least-square fit was performed on the experimental $L(E)$, following the expressions [7]

$$L(E) = \begin{cases} A_0 + \dfrac{B_0}{(E+Q)^{\frac{3}{2}}}, & Q < 0 \\ A_0 + \dfrac{B_0}{E^{\frac{3}{2}}}, & Q > 0 \end{cases} \qquad (3)$$

where Q represents the fusion Q-value of the system. The quantities A_0 and B_0, in Eq. 3, are free parameters, values of which were obtained from the least square fit. The data point at the lowest energy was not considered in the fitting procedure in case of ^{16}O+^{142}Ce because of probable presence of background events, as discussed earlier in Sec. 3. Using the extracted values of A_0 and B_0, $L(E)$ was extrapolated towards lower energy, which is shown in Fig. 3(a) and Fig. 4(a) (solid line) for ^{16}O+^{116}Cd and ^{16}O+^{142}Ce, respectively. In both cases, the extrapolated line intersects the $L_{\rm CS}(E)$ curve, which denotes probable onset of fusion hindrance. The threshold energy ($E_{\rm S}$) and the logarithmic slope at the threshold energy ($L_{\rm S}$), at which onset of hindrance occurs are given, respectively, by the x and y-coordinates of the intersection point. These values were compared with the empirical values $E_S^{emp} = \left(0.495\zeta/L_s^{emp}\right)^{2/3}$ and $L_S^{emp} = 2.33 + 580/\zeta$ [10, 15]. The results of the symmetric systems with similar ζ that were already reported, *viz.*, ^{32}S+^{48}Ca [31] and ^{36}S+^{48}Ca [30] were compared with results of ^{16}O+^{116}Cd. $L(E)$ for these systems are shown in Figs. 3(b) and Fig. 3(c). Similar comparisons were made between the results of symmetric

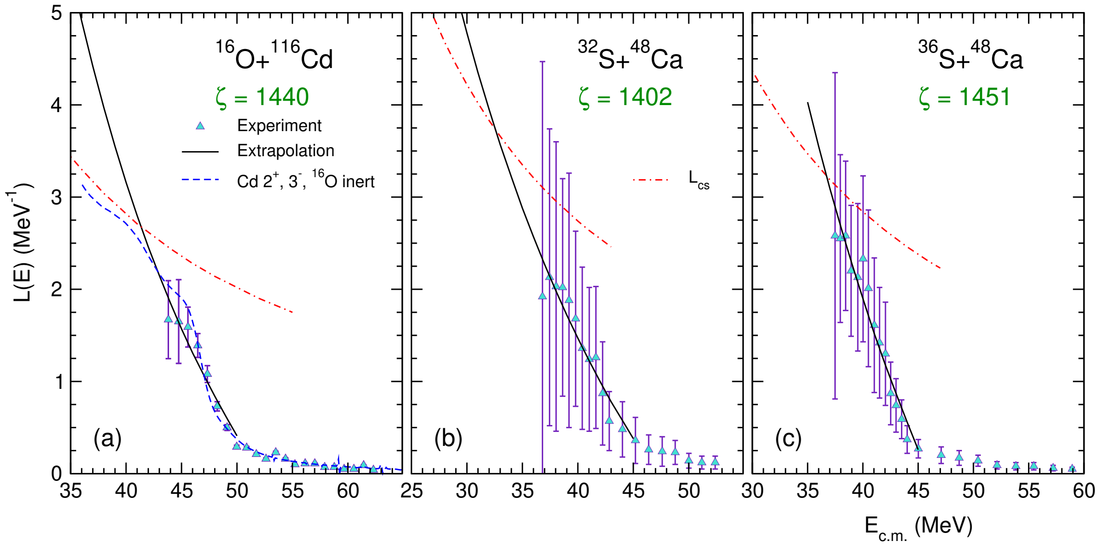

Figure 3: Logarithmic slope for the asymmetric system (a) ^{16}O+^{116}Cd, compared with the same of the symmetric systems (b) ^{32}S+^{48}Ca and (c) ^{36}S+^{48}Ca, having similar values of ζ. $L(E)$ extracted from the CC calculations has also been shown in panel (a).

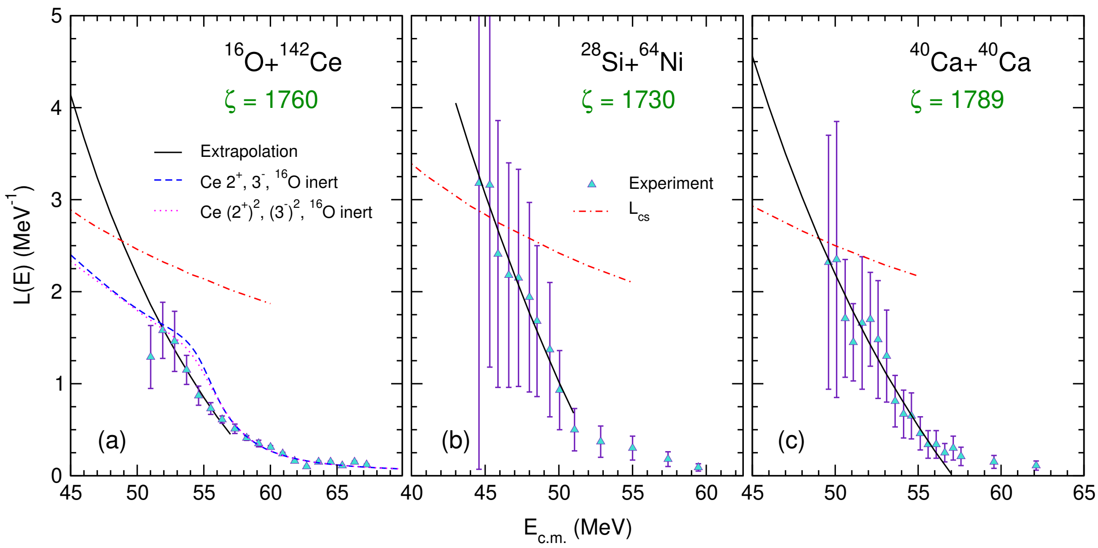

Figure 4: Logarithmic slope for the asymmetric system (a) ^{16}O+^{142}Ce, compared with the same of symmetric systems (b) ^{28}Si+^{64}Ni and (c) ^{40}Ca+^{40}Ca having similar values of ζ. $L(E)$ extracted from the CC calculations have also been shown in panel (a).

systems ^{28}Si+^{64}Ni [32] (Fig. 4(b)), ^{40}Ca+^{40}Ca [33] (Fig. 4(c)) and that of ^{16}O+^{142}Ce.

Parameters extracted from extrapolation *i.e.*, E_S and L_S along with E_S^{emp} and L_S^{emp} for all the systems mentioned above are tabulated in Table 2. The threshold energy of hindrance for the system ^{16}O+^{116}Cd is found to lie about 2 MeV below the lowest energy (E = 43.06 MeV), at which measurement was performed. For the system ^{16}O+^{142}Ce, it lies about 1 MeV below the lowest energy (E = 50.33 MeV). The system ^{32}S+^{48}Ca was reported to show absence of hindrance due to the presence of PQNT channels, which is evident from the Table 2 where the estimated E_S is much lower than the empirical value. The empirical relation has been found to be quite accurate for systems with closed-shell nuclei. The actual threshold tend to move towards energy lower than the empirical threshold with increase in number of nucleons beyond the closed shell.

Logarithmic slopes extracted from CC results for both the systems are also shown in Fig. 3(a) and Fig. 4(a). The curves run nearly parallel to the $L_{CS}(E)$ curve above.

3.4 Astrophysical S-factor

The astrophysical S-factors were determined using the relation

$$S(E) = E\sigma \exp\{[2\pi(\eta(E) - \eta(E_S))]\} \quad (4)$$

where $\eta(E)$ is the Sommerfeld parameter. The variation of S-factor with respect to E for the systems ^{16}O+^{116}Cd and

Table 2: Comparison between experimentally determined threshold energy (E_S) and logarithmic slope at the threshold energy (L_S) with their empirical counterparts E_S^{emp} and L_S^{emp}, which are functions of the ζ-parameter, for asymmetric and symmetric systems with similar values of ζ.

System	ζ	E_S (MeV)	E_S^{emp} (MeV)	L_S (MeV^{-1})	L_S^{emp} (MeV^{-1})
^{16}O+^{116}Cd	1440	41.34	40.85	2.68	2.73
^{32}S+^{48}Ca	1402	32.55	40.03	3.74	2.74
^{36}S+^{48}Ca	1451	36.71	41.06	3.23	2.73
^{16}O+^{142}Ce	1760	48.89	47.41	2.55	2.66
^{28}Si+^{64}Ni	1730	45.60	46.97	2.78	2.66
^{40}Ca+^{40}Ca	1789	49.03	48.16	2.58	2.65

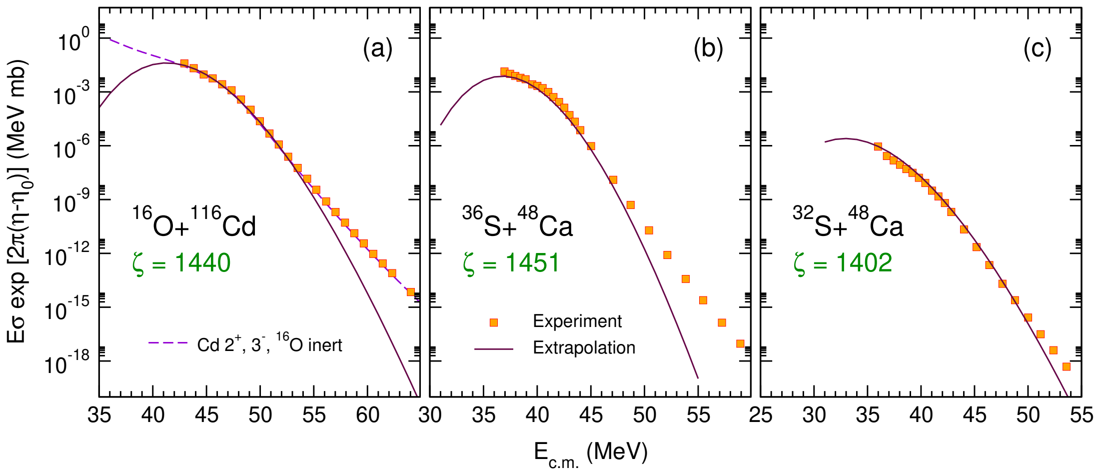

Figure 5: S-factor for the asymmetric system (a) ^{16}O+^{116}Cd, compared with the same of symmetric systems (b) ^{32}S+^{48}Ca and (c) ^{36}S+^{48}Ca having similar values of ζ. S-factor extracted from the CC calculations have also been shown in panel (a).

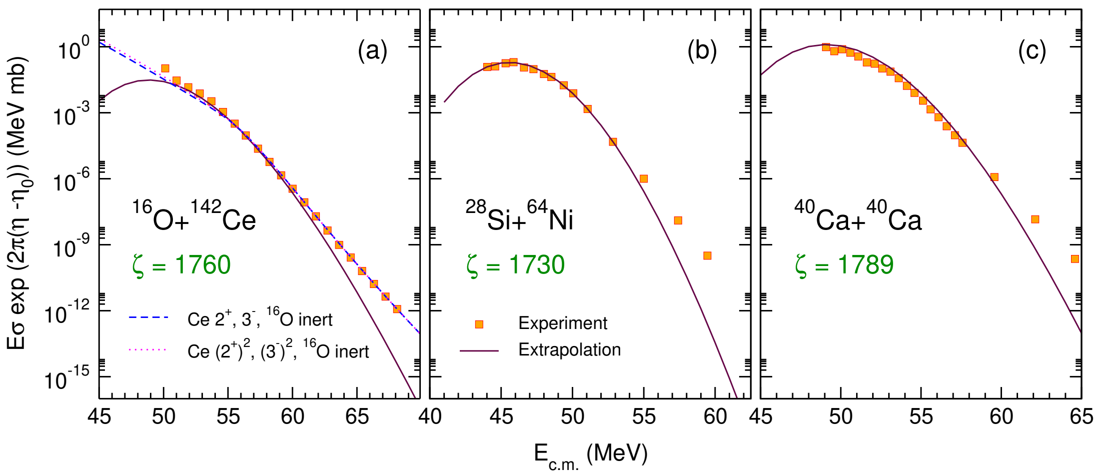

Figure 6: S-factor for the asymmetric system (a) ^{16}O+^{142}Ce, compared with the same of symmetric systems (b) ^{28}Si+^{64}Ni and (c) ^{40}Ca+^{40}Ca having similar values of ζ. S-factor extracted from the CC calculations have also been shown in panel (a).

^{16}O+^{142}Ce are shown in Fig. 5(a) and Fig. 6(a), respectively. It is observed from the figures that the S-factors, extracted from experimental σ_{fus} and CC calculations, rise monotonously. Thus presence of fusion hindrance cannot be inferred in the absence of a maximum for both systems.

In order to extrapolate the S-factor to energies beyond the lowest E_{lab}, empirical fusion cross-sections, for systems with a negative Q-value, were calculated using the relation [7]

$$\sigma(E) = \sigma_s \frac{E_s}{E} \exp\left\{\left[A_0 (E - E_s) - \frac{2B_0}{\sqrt{E_s + Q}} \left(\sqrt{\frac{E_s + Q}{E + Q}} - 1\right)\right]\right\} \tag{5}$$

The S-factors calculated from the empirical fusion cross sections are shown in Fig. 5(a) and Fig. 6(a) (solid line) for ^{16}O+^{116}Cd and ^{16}O+^{142}Ce, respectively. The quantity σ_s in Eq. (5), which is a normalization factor, was calculated using the σ_{fus} value at the lowest E_{lab}. For ^{16}O+^{142}Ce, the data point at the second lowest energy was used for this purpose. The maxima in the extrapolated S-factors are observed at $E \simeq 41$ MeV and $E \simeq 49$ MeV for ^{16}O+^{116}Cd and ^{16}O+^{142}Ce, respectively, which match quite closely with the values of E_S mentioned in Table 2. Fig. 5 also includes the S-factors extracted via extrapolation of data points for ^{32}S+^{48}Ca and ^{36}S+^{48}Ca. Similarly, Fig. 6 shows comparison of the system ^{16}O+^{142}Ce with the symmetric systems ^{28}Si+^{64}Ni and ^{40}Ca+^{40}Ca.

4 Conclusions

Fusion excitation functions were measured for the asymmetric systems ^{16}O+^{116}Cd and ^{16}O+^{142}Ce down to $\simeq 14\%$ below the barrier. CC calculations, with couplings to low-lying excited states of the heavier collision partner in each case, were able to reproduce the measured σ_{fus} fairly well in the range of E_{lab} explored in this work. Experimental $\mathcal{D}$s, extracted from the data by two different methods for both systems, had a smooth form with a single peak. $\mathcal{D}$s obtained from CC results also had similar structure. We further extracted the logarithmic slopes from the experimental σ_{fus}. Upon extrapolation of $L(E)$ beyond the lowest E_{lab} at which measurements were performed, an intersection with the $L_{CS}(E)$ curve was observed. The threshold energy for onset of fusion hindrance, indicated by the intersecting point, matched with the empirical value of the threshold energy for both the asymmetric systems. Astrophysical S-factors were calculated for both systems and the same were extrapolated to lower energies. A maximum was observed in each case. These observations pointed to the likely presence of fusion hindrance in both reactions. Additionally, our results for the asymmetric systems were compared with the same from symmetric systems having similar values of the system parameter ζ. Our systematic investigation led to the conclusion that fusion hindrance was a common feature in all these systems, irrespective of the entrance channel mass asymmetry. However, extending the measurements towards lower energies would be crucial to assert our conclusions.

Acknowledgements
One of the authors (R.B.) acknowledges the Council of Scientific and Industrial Research (CSIR), New Delhi for financial support via grant no. CSIR/09/760(0030)/2017-EMR-I. The authors are thankful to the Pelletron crew of IUAC for providing pulsed beam with requisite specifications and the staff of the IUAC Target Development Laboratory for excellent support in preparing the enriched target films. Discussions with Dr. Md. Moin Shaikh in early stages of the work are thankfully acknowledged.

References

[1] M. Dasgupta *et al.*, Annu. Rev. Nucl. Part. Sci. **48**, 401 (1998).
[2] B. B. Back *et al.*, Rev. Mod. Phys. **86**, 317 (2014).
[3] G. Montagnoli and A. M. Stefanini, Eur. Phys. J. A **53**, 169 (2017).
[4] G. Montagnoli and A. M. Stefanini, Eur. Phys. J. A **59**, 138 (2023).
[5] K. Hagino and N. Takigawa, Prog. Theo. Phys. **128**, 1061 (2012).
[6] C. L. Jiang *et al.*, Phys. Rev. Lett. **89**, 052701 (2002).
[7] C. L. Jiang *et al.*, Eur. Phys. J. A **57**, 235 (2021).
[8] C. L. Jiang *et al.*, Phys. Rev. Lett. **93**, 012701 (2004).
[9] C. L. Jiang *et al.*, Phys. Rev. C **71**, 044613 (2005).
[10] C. L. Jiang *et al.*, Phys. Rev. C **73**, 014613 (2006).
[11] A. Shrivastava *et al.*, Phys. Lett. B **755**, 332 (2016).
[12] C. L. Jiang *et al.*, Phys. Lett. B **640**, 18 (2006).
[13] C. L. Jiang *et al.*, Phys. Rev. C **78**, 017601 (2008).
[14] C. L. Jiang *et al.*, Phys. Rev. C **81**, 024611 (2010).
[15] H. Esbensen and C. L. Jiang, Phys. Rev. C **79**, 064619 (2009).
[16] A. M. Stefanini *et al.*, Phys. Rev. C **96**, 014603 (2017).
[17] C. L. Jiang *et al.*, Phys. Rev. C **79**, 014604 (2004).
[18] Ş. Mişicu and H. Esbensen, Phys. Rev. Lett. **96**, 112701 (2006).
[19] Ş. Mişicu and H. Esbensen, Phys. Rev. C **75**, 034606 (2007).
[20] T. Ichikawa *et al.*, Phys. Rev. C **75**, 057603 (2007).
[21] T. Ichikawa *et al.*, Phys. Rev. Lett. **103**, 202701 (2009).
[22] T. Ichikawa, Phys. Rev. C **92**, 064604 (2015).

[23] C. Simenel *et al.*, Phys. Rev. C **95**, 031601(R) (2017).
[24] M. Dasgupta *et al.*, Phys. Rev. Lett. **99**, 192701 (2007).
[25] A. Shrivastava *et al.*, Phys. Rev. Lett. **103**, 232702 (2009).
[26] S. Bhattacharjee *et al.*, Phys. Rev. C **104**, 054607 (2021).
[27] A. Shrivastava *et al.*, Phys. Rev. C **96**, 034620 (2017).
[28] A. Pakou *et al.*, Phys. Rev. C **102**, 031601(R) (2020).
[29] Md. Moin Shaikh *et al.*, J. Phys. G: Nucl. Part. Phys. **45**, 095103 (2018).
[30] A. M. Stefanini *et al.*, Phys. Rev. C **78**, 044607 (2008).
[31] G. Montagnoli *et al.*, Phys. Rev. C **87**, 014611 (2013).
[32] C. L. Jiang *et al.*, Phys. Lett. B **640**, 18 (2006).
[33] G. Montagnoli *et al.*, Phys. Rev. C **85**, 024607 (2012).
[34] A. K. Sinha *et al.*, Nucl. Instrum. Methods A **339**, 543 (1994).
[35] Rohan Biswas *et al.*, Nucl. Instrum. Methods A **1046**, 167696 (2023).
[36] Rohan Biswas *et al.*, Vacuum **188**, 110159 (2021).
[37] S. Nath *et al.*, Phys. Rev. C **81**, 064601 (2010).
[38] S. Nath, Comput. Phys. Commun. **179**, 492 (2008); *ibid* **180**, 2392 (2009).
[39] N. Rowley *et al.*, Phys. Lett. B **254**, 25 (1991).
[40] C. L. Jiang and B. P. Kay, Phys. Rev. C **105**, 064601 (2022).
[41] K. Siwek-Wilczyńska and J. Wilczyński, Phys. Rev. C **69**, 024611 (2004).
[42] K. Hagino *et al.*, Comput. Phys. Commun. **123**, 143 (1999).
[43] B. Pritychenko, M. Birch, B. Singh, M. Horoi, At. Data Nucl. Data Tables **107**, 1 (2016).
[44] T. Kibédi and R. H. Spear, At. Data and Nucl. Data Tables **80**, 35 (2002).